Numerical study of a lattice-gas model for micellar binary solutions

Smaîne Bekhechi and Abdelilah Benyoussef
Laboratoire de Magnétisme et de Physique des Hautes Energies, Département de Physique, Faculté des Sciences, Boîte Postale 1014, Rabat, Morocco

Najem Moussa
LPTMC Département de Physique, Faculté des Sciences et Techniques, Boîte Postale 509, Boutalamine, Errachidia, Morocco
(Received 29 September 1998)

Two nonperturbative methods such as transfer-matrix finite-size scaling and Monte Carlo simulations are used to investigate the multicritical behavior of a lattice-gas model proposed by Shnidman and Zia [J. Stat. Phys **50**, 839 (1988)] for studying the micellar binary solutions of water and amphiphile. The phase diagrams are obtained in both the magnetic field-temperature (H,T) and amphiphile density temperature (ρ_s,T) for different values of competing interactions (K_0 and K_1) and in the presence of the attraction interaction intermicellar parameter (J). Our nonperturbative results are compared with previous mean-field ones. Both methods confirm the absence of the rarefied micelle at high temperature as found previously by mean-field calculations. Also our phase diagrams present transitions of first- and second-order transitions linked by tricritical and multicritical points of higher order. Finally, with the use of finite-size-scaling ideas, the critical exponents have been calculated. Our results show that this model has a nonuniversal behavior that belongs to the XY model with cubic anisotropy for a certain range of interactions parameters and a universal behavior that belongs to the $d=2$ Ising model.

I. INTRODUCTION

In recent years great effort has been made in experimental and theoretical physics to understand the behaviors of phase diagrams of amphiphilic systems.[1–16] The amphiphile or a surfactant molecule is made of two parts having opposing natures: one is the water soluble (hydrophilic) and the other is oil soluble (hydrophobic). The hydrophilic and hydrophobic parts are linked together by a chemical bond and consequently cannot phase separate as they would if the two parts were free.

In general, when such molecules are put in water they prefer the (water-air) surface, and the hydrophilic ''heads'' and hydrophobic ''tails'' lie, respectively, in and out of the water. Indeed, the amphiphile molecules in water try to arrange themselves as to only expose their polar head groups to the water molecules. For small amount of amphiphiles, they practically all lie at the interface and as a consequence, the (liquid-vapor) surface tension decreases as the concentration of amphiphiles increases. Then, at a certain concentration [the critical micellar concentration (CMC)] the surface tension levels off and remains nearly constant. A study of this phenomena[8] confirms that the added amphiphiles molecules no longer go preferentially to the surface but rather go into solution in bulk of the acqueous phase. Then the molecules organize themselves as small aggregates ''micelles'' that are often globular in shape, the tails comprising the interior and the heads coating the surface and this leads to an isotropic micellar solution ''I.''

In both the very low-concentration regime, where most of the added molecules are at the surface, and in the higher concentration case, where aggregates are formed, the physical phenomenon responsible for such behavior is referred to as the hydrophobic effect and is due to a subtle balance between intermolecular energies and entropies. In particular, when the amphiphile is wholly immersed in water, the molecules again try to reduce the area of contact with water and the network of hydrogen bonds between water molecules reconstructs itself to avoid the region occupied by the hydrocarbon. This constraint on the local structure of water decreases the entropy near the hydrocarbon, and it results in an increase in the free energy of the system.[8] For the binary amphiphilic systems, the aggregation of molecules induces equilibrium processes controlled by intermoleculer and interaggregates forces.[9] For concentrations of amphiphiles that exceed the CMC a large variety of structures occur. Micellar aggregates appear in various shapes and sizes. Upon increasing further the concentration of amphiphiles, long-range ordered phases may appear, such as lamellar or hexagonal cubic states called; ''the lyotropic liquid crystals.''

This suggests a classification of the aggregates into three general categories as follows: (1) globular aggregates (zero dimension) where a spherical micelle is a prototype of this class; (2) globular aggregates (one dimension) where a cylindrical micelle is the typical example of this class; (3) bilayers (two dimensions) where a disklike aggregate is an example of this class. The choice among all the possible shapes is determined by interactions between the hydrophilic head groups and geometric packing constraints on the hydrophobic tails, but the transition from one shape to another may be obtained by changing either the temperature or the amphiphile concentration or by adding a third component.[6]

Among the experiments study of the structure of the micellar aggregates are the important work of Debye and Anacker[17] that involved light-scattering studies of a series n-alkyl trimethyl ammonium bromides $[C_nH_{2n+1}N(CH_3)_3^+Br]$. It was concluded that, above the CMC aggregates appear as the dominant species and the mi-

celles underwent a transition from spherical to rodlike aggregates upon increase in amphiphile concentration. The phase diagram of water and $C_{12}E_5$ system [i.e., $C_{12}H_{25}(OCH_2CH_2)_5OH$] that represents such phenomena is reproduced by Strey *et al.*[13]

Several models of the binary mixtures of an amphiphile and water have been proposed in order to reproduce the phases observed experimentally.[3,4,18] On the one hand, Gompper and Schick[4] and Matsen and Sullivan[3] have exhibited within mean-field theory a two-phase coexistence between water-rich and amphiphile-rich phases, but at higher temperatures there is a single disordered phase. On the other hand, within a microscopic approach, Shnidman and Zia[19] have proposed a lattice-gas model, based on constructing a coarse-grained representation of different types of aggregates occurring in micellar binary solutions (MBS's) in terms of Ising variables. One introduces on a lattice site (i,j) the Ising variable satisfying $s_{i,j}=+1$ for a micellar section and $s_{i,j}=-1$ describes a region, of comparable size, predominantly occupied by a solvent. A single $+1$ spin completely surrounded by -1 spins, is identified with a globular micelle, and a linear chain of $+1$ spins surrounded by -1 spins corresponds to a rodlike micelle. Finally, a spin $+1$ at the end of a chain of $+1$ spins surrounded by -1 spins, is called an end cap.[19]

The two dimensional version of this model has been studied within perturbation theory[20] and mean-field approximation[21] (MFA) which yielded rich phase diagrams, in the parameter space T and h and J, with multicritical points of higher order. For the three-dimensional version of this model, the phase diagrams obtained within MFA (Ref. 22) describe qualitatively all the states observed experimentally except the lamellar phase. In order to fill the absence of this latter phase, another term has been added to the Shnidman-Zia Hamiltonian, which reproduce this lamellar phase. The phase diagrams obtained by MFA (Ref. 23) for this new Hamiltonian show all the lyotropic phases observed experimentally.

Transfer-matrix methods and Monte Carlo simulations applied to finite systems and finite-size-scaling theory have been used with great success to study the critical properties of Ising models[24–27] especially at low spatial dimensions. As we know these two approaches[28–30] include the correlated fluctuations, which are very strong in two dimensions, and which are ignored by the mean-field approximation. So it is important to understand this model by using these two powerful nonperturbative methods such as transfer-matrix finite-size-scaling (TMFSS) calculations and Monte Carlo simulations (MC). The objectives of this study are (i) to determine the global phase diagrams in the H-T and ρ_s-T planes, (ii) to compare our results with the previous MFA ones,[21] (iii) to discuss the critical properties of this rich model from the exponents calculations.

The remainder of this paper is organized as follows: In Sec. II, we describe the model and the ground-state diagrams. Section III contains the formalism of the transfer-matrix finite-size-scaling method, and the Monte Carlo simulations are described in Sec. IV. Our numerical results for the phase diagrams and the critical exponents are presented in Sec. V. Finally, Sec. VI presents a summary and a conclusion.

II. MODEL AND GROUND STATE

The Hamiltonian of the two-dimensional proposed model is a sum of three terms:

$$H=H_k+H_j+H_h,$$

where H_k is effective at the intramicellar length scale, representing many-body interactions responsible for self-association and controlling the size and shape distribution of aggregates, and H_j describes an effective short-range coupling between the aggregates at a larger intermicellar length scale. Finally, H_h represents the usual chemical potential for controlling the concentration of amphiphiles (micelles) in the grand canonical formulation.

We assign negative energies $-K_0$ and $-K_1$, respectively, for the formation of a spherical micelle and a rodlike micelle. For an end cap, the average $-(K_0+K_1)/2$ is chosen.

To write H explicitly, it is convenient to use the lattice-gas variables:

$$t_{i,j}=(1+\sigma_{i,j})/2, \quad S_{i,j}=(1-\sigma_{i,j})/2.$$

For further convenience, we define the bilinear products:

$$u_{i,j}=t_{i-1},t_{i+1,j},$$

$$v_{i,j}=S_{i-1,j}S_{i+1,j},$$

$$w_{i,j}=t_{i-1,j}S_{i+1,j}+S_{i-1,j}t_{i+1,j}$$

and similar ones with $i\leftrightarrow j$. In terms of these operators, H is

$$H=-K_0\sum\ tv_iv_j-\tfrac{1}{2}(K_0+K_1)\sum\ t(w_iv_j+v_iw_j)$$
$$-K_1\sum\ t(u_iv_j+v_iu_j)-J\sum\ S(u_i+u_j)-h\sum\ (t-s), \tag{1}$$

where we have suppressed all except the underlined indices and the summations are over all sites indices.[19]

The Hamiltonian H is transformed in terms of Ising variables, to the form:

$$-H=J_1\sum_1\ \sigma_i+J_2\sum_2\ \sigma_i\sigma_j+J_3\sum_3\ \sigma_i\sigma_j+J_4\sum_4\ \sigma_i\sigma_j$$
$$+J_5\sum_5\ \sigma_i\sigma_j\sigma_k+J_6\sum_6\ \sigma_i\sigma_j\sigma_k+J_7\sum_7\ \sigma_i\sigma_j\sigma$$
$$+J_8\sum_8\ \sigma_i\sigma_j\sigma_k\sigma_l+J_9\sum_9\ \sigma_i\sigma_j\sigma_k\sigma_l$$
$$+J_{10}\sum_{10}\ \sigma_i\sigma_j\sigma_k\sigma_l\sigma_m. \tag{2}$$

The sum runs over all the spins in different sites, bonds and loops, see Fig. 1(a), and all the interactions parameters are given by

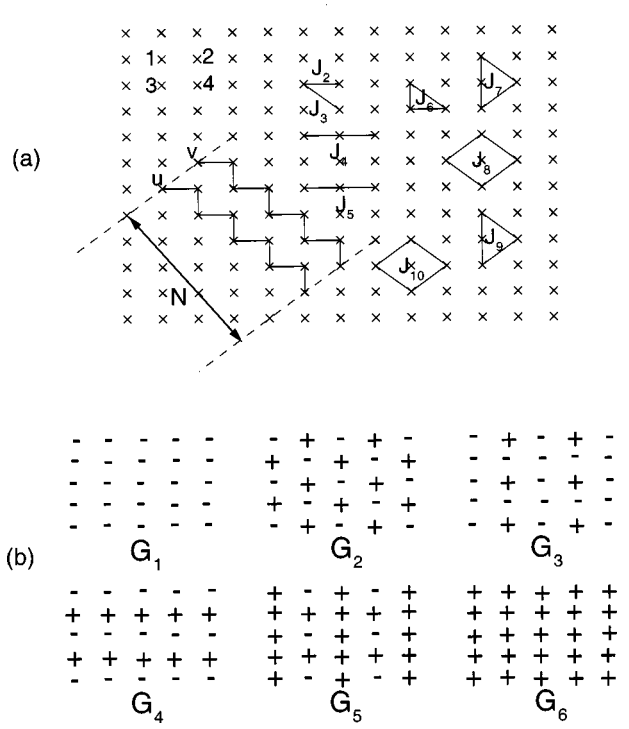

FIG. 1. (a) Lattice-gas model on a square lattice, shown by crosses, with pairwise interactions J_2, J_3, J_4; three-particle interactions J_5, J_6, J_7; four- and five-particle interactions J_8, J_9 and J_{10}, respectively. The zigzag-shaped layers u and v into which the lattice is decomposed for transfer-matrix calculations are indicated by light lines. N design the length of the strip width ($N=9$ in the figure). In the upper left-hand corner are shown the numbers 1, 2, 3, 4, which labels the four sublattices that define the Monte Carlo order parameters. (b) The states which can be realized as ground states with the Hamiltonian (1). The disordered states G_1 and G_6, and the ordered states G_2, G_3, G_4, G_5, which can be reached by a second-order phase transition (Refs. 43 and 44) (see the text for the equivalent Ising formulation).

$$J_1=(-5K_0+8J+32h)/32,$$

$$J_2=-(4K_0+2K_1+8J)/32, \quad J_3=(2K_0-4K_1)/32,$$

$$J_4=(K_0+2K_1+4J)/32,$$

$$J_5=(K_0+2K_1-4J)/32, \quad J_6=(K_0-2K_1)/32,$$

$$J_7=J_8=K_1/32, \quad J_9=J_{10}=-K_0/32,$$

where K_0, K_1, and J are positive. We note that the model describing the physical situation corresponds to positive values of J.

Finally the amphiphile density is given by

$$\rho_s=\langle t_{i,j}\rangle=\tfrac{1}{2}(1+M), \tag{3}$$

where M is the total magnetization of the system.

In order to discuss the ground state of this model, it is useful to introduce the ground states of the system, [20] which are defined as follows, see Fig. 1(b). We denote by G_1 the water ground state (g.s.) which is in the Ising formulation the disordered state $(1\times1)^{0}_{-}$ [where the subscript $(\_)$ designs that the majority of the spins are down $S_i=-1$ and the upper one refer to the associated density ρ_s from Eq. (3)], G_2 the spherical micelles (g.s.) or the antiferromagnetic state $c(2\times2)^{0.5}_{-}$, G_3 the rarefied spherical micelles (g.s.) or the degenerate structure $(2\times2)^{0.25}_{-}$, G_4 the infinite rodlike micelles (g.s.) or the superantiferromagnetic phase (SAF) $(2\times1)^{0.5}_{-}$, G_5 the reversed micelles (g.s.) or the degenerate structure $(2\times2)^{0.75}_{+}$, and G_6 the amphiphile (g.s.) which is the disordered state $(1\times1)^{1}_{+}$.

The phase diagrams at zero temperature of the system have been established elsewhere (see Refs. 20 and 21 for more details) in the plane (J,h) for all values of the parameters, K_0, K_1, such that $K_1>K_0$ and also for the case $K_1<K_0$.

III. TRANSFER-MATRIX FINITE-SIZE-SCALING (TMFSS) CALCULATIONS

Detailed description of the phenomenological finite-size-scaling method and transfer-matrix formalism on two-dimensional systems are given in Refs. 31, and 32. In order to limit the range of the Hamiltonian to only adjacent layers of the lattice and to accommodate all the interactions J_n, we define zigzag-shaped layers, as shown in Fig. 1(a). Also in our case only even values of N are considered to avoid the introduction of interfaces and to preserve the symmetries of all the ground states, the strip width N must be a multiple of 4 (we point out that in the case of the G_2 (g.s.) strip widths which are multiples of 2 could be used) and the system obeys periodic boundary conditions. So with $N'=N+4$ the Nightingale condition[13] for the determination of the critical point K_c becomes

$$\frac{\xi_N(K_c)}{N}=\frac{\xi_{N+4}(K_c)}{N+4}, \tag{4}$$

where $\xi_N(K)$ is the correlation length. The symbol K denotes the set of fields $K=(T,h)$. The nature of the transition (first order or continuous) is determined by examining the finite-size-scaling behavior of the persistence length $\tilde{\xi}$.[29,30,33,34] If the scaled persistence length $\tilde{\xi}/N$ on the transition line is a decreasing function of N then the transition is continuous, otherwise the transition is first order. This method has proven its accuracy for systems with short-range interactions that have simple eigenvalue spectrum. In general, when the interactions have long-range strengths, the eigenvalue spectrum becomes more complex to analyze, degeneracies and large finite-size effects may obscure the choice of the persistence length. An alternative method to identify a first-order transition, is to use the exponential divergence with N of the maximum value $\chi^{\max}$ of the nonordering susceptibility. Since this quantity depends only on the derivative of the largest eigenvalue of the system, it is more robust in the identification of first-order transition (see Refs. 35–37 for details and comparison).

The correlation length and the persistence length are obtained from the largest eigenvalues of the transfer matrix. In the transfer-matrix method, the lattice is approximated by an $N\times\infty$ lattice with periodic boundary conditions in the finite direction.

The full 2^N*2^N transfer matrix, which is not symmetric under transposition, can be block diagonalized using invari-

ance under two-step translation in the transverse direction. The G_1, G_2, and G_6 phases are symmetric under this operation, whereas the G_4 phase is antisymmetric and the G_3, G_5 states are of mixed symmetries. The symmetric and the antisymmetric blocks, T^S (700*700 for $N=12$) and T^A (698*698 for $N=12$), are the only blocks whose symmetries correspond to ordered phases. We diagonalized them with real antisymmetric (RAS) library routines (based on EISPACK routines) based on IBM 6000. The diagonalization results in four eigenvalues of interest. The largest eigenvalue of both T^S and the transfer matrix is λ_1^S. By virtue of the Perron-Frobenius theorem, it is positive and nondegenerate. The other three next eigenvalues are λ_2^S and λ_3^S, second- and third-largest eigenvalues of T^S, and λ_1^A, the largest eigenvalue of T^A. These four eigenvalues give rise to three important lengths:

$$\xi_1^S=(\ln|\lambda_1^S/\lambda_2^S|)^{-1} \tag{5}$$

is the largest length corresponding to T^S. It diverges exponentially with N in the G_2, G_4, G_3, and G_5 phases.

$$\xi_2^S=(\ln|\lambda_1^S/\lambda_3^S|)^{-1} \tag{6}$$

is the second largest length corresponding to T^S. It remains small and independent of N in the ordered phases, but peaks near the transitions.

And finally,

$$\xi_1^A=(\ln|\lambda_1^S/\lambda_1^A|)^{-1} \tag{7}$$

is the largest length corresponding to T^A. It diverges exponentially with N in the G_4 phase. We note that at the disorder to G_4 transition $\xi_1^A \cong \xi_1^S$, with ξ_1^A dominant.

The correlation length exponent ν is obtained following the argument of Nightingale.[31]

$$\nu^{-1}=\ln\left(\frac{N\partial\xi_N^{-1}(K_c)/\partial T}{(N+1)\partial\xi_{N+1}^{-1}(K_c)/\partial T}\right)[\ln(N/N+1)]^{-1}. \tag{8}$$

In order to have good estimates of ν we have made differentiation that are orthogonal to the phase boundaries. Finally the total magnetization is computed from the Gibbs free-energy per spin[32] as: $M=-\partial g_1(T,H)/\partial(H)$ with $g_1(T,H)=-(T/N)\ln|\lambda_1^S|$.

IV. MONTE CARLO SIMULATION

We have performed Monte Carlo simulations to complement transfer-matrix results. The system studied is $L*L$ square lattice with even L, containing $N=L^2$ spins, and we use the well-known Metropolis algorithm[38] with periodic boundary conditions to update the lattice configurations over one sweep of the entire N spins of the lattice [one Monte Carlo step (MCS)]. Counted after the system reaches thermal equilibrium. To calculate the physical quantities, we decompose the lattice into four sublattices that are appropriate for the description of all the states. Our program calculates the internal energy, the specific heat,

$$U=\frac{1}{L^2}\langle H\rangle, \quad C=\frac{\beta^2}{L^2}[\langle H^2\rangle-\langle H\rangle^2] \tag{9}$$

with $\beta=1/k_BT$ (where k_B is the Boltzmann constant) and the sublattice and total magnetizations, M_α ($\alpha=1,2,3,4$) and M, respectively, by

$$M_a=\frac{4}{L^2}\left\langle\sum_{i\in\alpha}\sigma_i\right\rangle, \quad \alpha=1,2,3,4; \quad M=\frac{1}{L^2}\left\langle\sum_i\sigma_i\right\rangle. \tag{10}$$

We also measured the order parameters defined as

$$M_{G2}=[M_1+M_4-(M_2+M_3)]/4. \tag{11}$$

Is the order parameter associated to the G_2 phase (antiferromagnetic structure). The order parameter of the G_4 phase (superantiferromagnetic SAF structure), has two components defined as

$$M_{G4}^1=[M_1+M_2-(M_3+M_4)]/4,$$

$$M_{G4}^2=[M_1+M_3-(M_2+M_4)]/4. \tag{12}$$

Thus the order parameter is defined from the root mean square[39] by

$$M_{G4}=[(M_{G4}^1)^2+(M_{G4}^2)^2]^{1/2}. \tag{13}$$

Finally, for the G_3 and G_5 structures, the order parameter has four components to be used;

$$M_{G5}^1=[M_1+M_2+M_3-M_4]/4,$$

$$M_{G5}^2=[M_2+M_3+M_4-M_1]/4,$$

$$M_{G5}^3=[M_3+M_4+M_1-M_2]/4,$$

$$M_{G5}^4=[M_4+M_1+M_2-M_3]/4. \tag{14}$$

And the corresponding root-mean-square order parameter is

$$M_{G5}=\left[\sum_{\alpha=1}^{4}(M_{G5}^\alpha)^2\right]^{1/2}. \tag{15}$$

We shall find useful the measurement of fluctuations (variance of the order parameter) and the Binder cumulant in the observable O defined by

$$\chi_0=\beta L^2(\langle O^2\rangle-\langle O\rangle^2)$$

$$U_L=1-\frac{\langle O^4\rangle_L}{3\langle O^2\rangle_L^2}, \tag{16}$$

where O designs the sublattice and total magnetizations and the order parameters as defined above.

Finally, we will use finite-size-scaling theory[37,39,40] to analyze our results. Following this approach, in the neighborhood of the infinite critical point T_c, and by using the scaled variable $x=tL^{1/\nu}$ ($t=|1-T/T_c|$), the above quantities obey for sufficiently large L;

$$M_L(T)=L^{-\beta/\nu}f(x),$$

$$\chi_L T(T)=L^{\gamma/\nu}g(x),$$

$$U_L(T)=U_0(x), \tag{17}$$

where in the limit of $t \to 0$, $x \to \infty$, $f(x) \to Bx^{\beta}$, and $g(x) \to Cx^{-\gamma}$, so that the infinite lattice critical behavior is recovered. If we derive the third equation of (17) with respect to the temperature T, we obtain the scaling relation,

$$U_L'(T) = L^{1/\nu} U_0'(x), \tag{18}$$

so that $U_L'(T_c) = L^{1/\nu} U_0'(0)$. Then we can find the critical exponent ν from the log-log plot of $U_L'(T_c)$ versus L.

V. RESULTS AND DISCUSSION

A. Phase diagrams

For finite temperature, all the phase diagrams in the (h,T) and (ρ_s,T) planes are obtained by transfer-matrix finite-size-scaling calculations with $N/N' = \frac{4}{8}$ and $\frac{8}{12}$. For the Monte Carlo data, lattices of sizes $8 < L < 128$, but most of the data are represented with $L = 40$. Hereafter we will discuss only phase diagrams that are different from those of mean-field ones.

(i) In the case $K_1 \geqslant K_0$ and $0 \leqslant J \leqslant K_1 - K_0$, $(K_1/K_0 = 2.0,\ J/K_0 = 0.5)$, the phase diagram in the (h,T) plane is obtained by both TMFSS calculations and MC simulations, as shown in Fig. 2(a). As seen from Fig. 2(a), at high temperature, there are two lines of continuous order-disorder transitions, $G_4 \leftrightarrow G_1$ and $G_5 \leftrightarrow G_6$. By decreasing the temperature, these transitions change to first order, resulting in two tricritical points C_1 $(2.38 \pm 0.001,\ 1.2 \pm 0.1)$ and C_3 $(-1.247 \pm 0.001,\ 0.4 \pm 0.1)$. These two ordered structures G_4 and G_5 are separated, in the neighborhood of $H = 0.0$, by lines of first- and second-order transitions at low and high temperatures respectively, and meeting at a tricritical point C_2 $(-0.038 \pm 0.001,\ 0.5 \pm 0.04)$. We also note in the phase diagram, the existence of a multicritical point B[3] where the three continuous lines intersect. To determine the critical points we have, on the one hand, for the $N/N' = 4/8$ and 8/12 TMFSS calculations, used the Nightingale criterion (4) of the correlation lengths, ξ_1^S for $G_5 \leftrightarrow G_6$ and ξ_1^A for $G_4 \leftrightarrow G_1$ (see Sec. III), whereas the nature of the transition is found from the behavior of the scaled persistence length ξ_2^S. The order-order critical points and the nature of the transitions have been determined from the persistence length[30] and the non-ordering susceptibility where the critical fields are given from peaks in these two quantities; the results obtained by both of these methods are consistent with each other. On the other hand, for the MC simulations, the data were obtained for a lattice of size $L = 40$ and 100 000 MCS after 50 000 sweeps had been discarded for thermal equilibrium. The second-order phase boundaries were obtained from peaks in the specific heat and along these boundaries neither hysteresis nor discontinuities in the order parameters or the internal energy was observed. Along the first-order lines strong hysteresis was observed when crossing this line in the H direction and it is located by using the mixed-start technique.[28,30] The tricritical points were determined when the hysteresis disappears. We note that the tricritical points have not been determined with high precision by the MC simulations but we have applied the Nightingale (4) criterion to the persistence length,[24,26,33,34] which is more accurate. The results obtained within these two methods are consistent with each other, except in the neighborhood of $H = 0$ where finite-size effects were strong and could be eliminated by using large strip widths in the TM calculations and finite-size scaling with extrapolation of the results.[29,37] We have also determined from the $N/N' = 8/12$ TMFSS calculations the phase diagram in the (ρ_s,T) plane. The amphiphile density ρ_s has been computed at the field corresponding to the maximum susceptibility. Below the multicritical points the peak in the susceptibility is exceedingly sharp, and the amphiphile density jumps almost discontinuously. In Fig. 2(b), we see the existence of the isotropic micellar phase ''I_1'' at a low concentration of amphiphile. At low temperature, as we increase the amphiphile concentration we pass to the intermediate phase, which is a coexistence between the isotropic micellar solution and the infinite rodlike micellar solid phase ''G_4'' and then to a pure infinite rodlike micellar solid structure with long-range order. By increasing the amphiphile concentrations, we go through coexistences from, infinite rodlike micellar solid phase ''G_4'' with the inverted micellar structure ''G_5,'' and the inverted micellar structure with the iso-

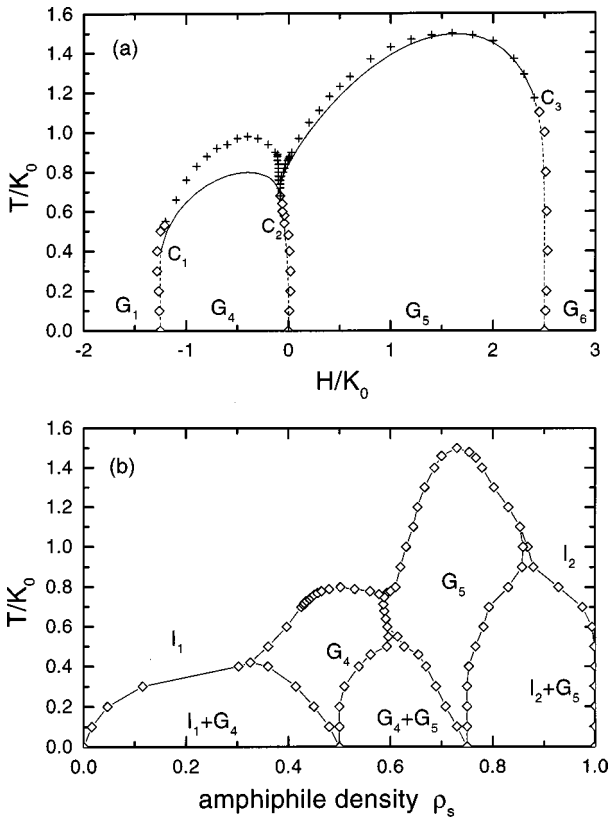

FIG. 2. The phase diagram of the model for $K_1 \geqslant K_0$ and $0 \leqslant J \leqslant K_1 - K_0$ (we use $K_1/K_0 = 2$ and $J/K_0 = 0.5$): (a) In the H,T plane, where the solid and dashed lines design second- and first-order transitions, respectively, which have been obtained by transfer-matrix finite-size-scaling calculations with $N/N' = \frac{8}{12}$. Monte Carlo results are also included for $L = 40$. $(+)$ represents critical points and $(\diamond)$ indicates first-order transitions. Three tricritical points, C_1, C_2, and C_3 occur. (b) In the equivalent ρ_s, T plane with the same parameters interaction as in (a), here all the data are obtained only with TMFSS calculations with $N/N' = \frac{8}{12}$. At low temperature the first-order transitions are indicated by coexistence regions. I_1 and I_2 are the isotropic micellar solution with low amphiphile density and the isotropic inverted micellar solution with amphiphile rich density, respectively.

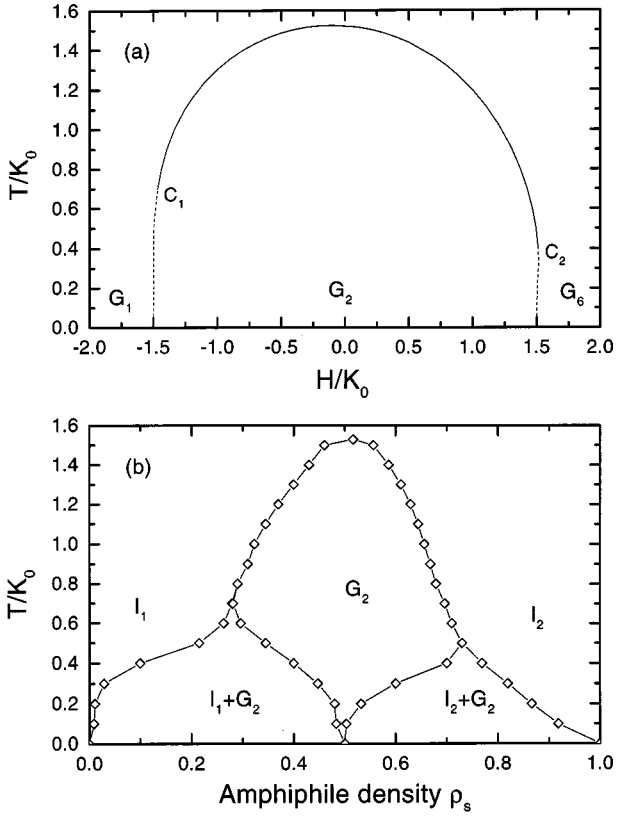

FIG. 3. The phase diagram of the model for $K_1 \leqslant K_0/2$ and $J>0$ (we use $K_1/K_0=0.25$ and $J/K_0=1.0$) based on TMFSS calculations with $\frac{8}{12}$ scaling in, (a) H,T plane where solid and dashed lines design second- and first-order transitions, respectively. Two tricritical points, C_1 and C_2, occur. (b) ρ_s, T plane where first-order transitions are indicated by coexistence regions at low temperature.

tropic inverted micellar solution (amphiphile rich phase) ''I_2'' to ''I_2'' that occurs at very high concentration. At high temperature, we pass from the isotropic micellar solutions ''I_1'' (water rich) to the inverted other one ''I_2'' (amphiphile rich) through the pure inverted micellar structure ''G_5.'' To compare our results in the (H,T) plane with previous MFA ones, we see that the latter approximation[21] yields large critical temperature and predicts another ordered phase (G_3 phase) at high temperature inside the G_5 phase, thus resulting in wrong topology of the phase diagram (see Refs. 39 and 41 for comparison between these two nonperturbative methods and MFA). For this purpose, we have spanned, in the H direction, all the region where this phase is suspected to be, from low-to-high temperatures in order to detect possible three peaks in the specific heat and the persistence length or the nonordering susceptibility. Only two peaks are observed in all the above quantities. Thus confirming the absence of the rarefied micelles G_3 at high temperature for these values of K_1/K_0 and J/K_0.

(ii) In the case $K_1 \leqslant K_0/2$ and $J>0$ ($K_1/K_0=0.25$, $J/K_0=1.0$) [Fig. 3(a)] in the (h,T) phase diagram there is only one ordered phase, the G_2 phase, which is separated at high temperature from the disordered phase by a line of critical points. This line meets, at two tricritical points C_1 (-1.466 ± 0.001, 0.7 ± 0.1) and C_2 (1.511 ± 0.001, 0.45 ± 0.03), lines of first-order transitions that separate the $G_1 \leftrightarrow G_2 \leftrightarrow G_6$ phases at low temperature. The critical points

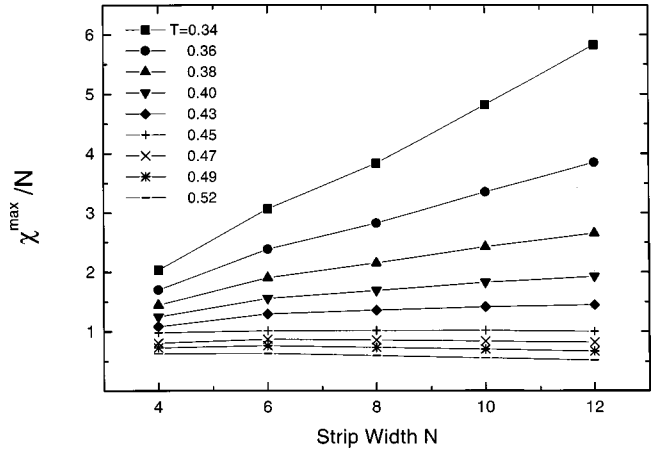

FIG. 4. Plots of the maximum of the nonordering susceptibility, $\chi^{\max}$ for different strip widths as obtained from transfer-matrix results, for $K_1/K_0=0.25$ and $J/K_0=1.0$. The data show at low temperature an exponential growth with N that signals a first-order transition, whereas no exponential growth with N is seen at higher temperatures indicating a second-order transition. A tricritical point is located at $H_t=1.51\pm0.01$ and $T_t=0.45\pm0.02$, where a linear behavior is seen.

have been obtained by TMFSS calculations with $N/N'=8/12$ and by applying the Nightingale criterion to the correlation length ξ_1^S. The ρ_s-T phase diagram generated with transfer-matrix scaling is shown in Fig. 3(b). On this phase diagram one observes that, at low temperatures, a phase transition from the isotropic micellar solutions (I_1 and I_2) to the coexistence of the (I_1+G_2) and (I_2+G_2) intermediates phases occurs. Moreover, at high temperatures, a direct phase transition occurs between the isotropic micellar solutions (I_1 and I_2) and the spherical micellar solid phase. This phase diagram has quite a resemblance with that found experimentally in the $C_{12}Na/H_2O$ system.[42]

Our results are similar but qualitatively better than those of MFA ones,[21] the main difference is the occurrence of a second tricritical point C_2 at high magnetic field. For this purpose we have also performed a transfer-matrix study of the scaling behavior of the maximum of the nonordering susceptibility $\chi^{\max}$, Fig. 4. We see that the tricritical point C_2 occurs at $T_t=0.45\pm0.03$ where a linear behavior is seen. MC simulations are also performed in the neighborhood of this value with $L=50$, 60 and our results show discontinuities (continuities) in the order parameter at $T=0.4$ ($T=0.5$) and are consistent with TMFSS calculations and confirm the existence of the tricritical point, and so a first-order transition at low temperature and a high positive magnetic field.

B. Critical behavior

In the preceding section we have concentrated on describing the general characteristics of phase diagrams. To discuss the critical behavior of this model, we have calculated by TMFSS the exponent ν from Eq. (8) with $N/N'=4/8$ and $N/N'=8/12$ for all the phase diagrams. For the $G_4 \leftrightarrow G_1$ and $G_5 \leftrightarrow G_6$ transitions, Fig. 2(a), we have also preformed a detailed MC simulations with finite-size-scaling analysis of the data to extract the exponents and so the universality of

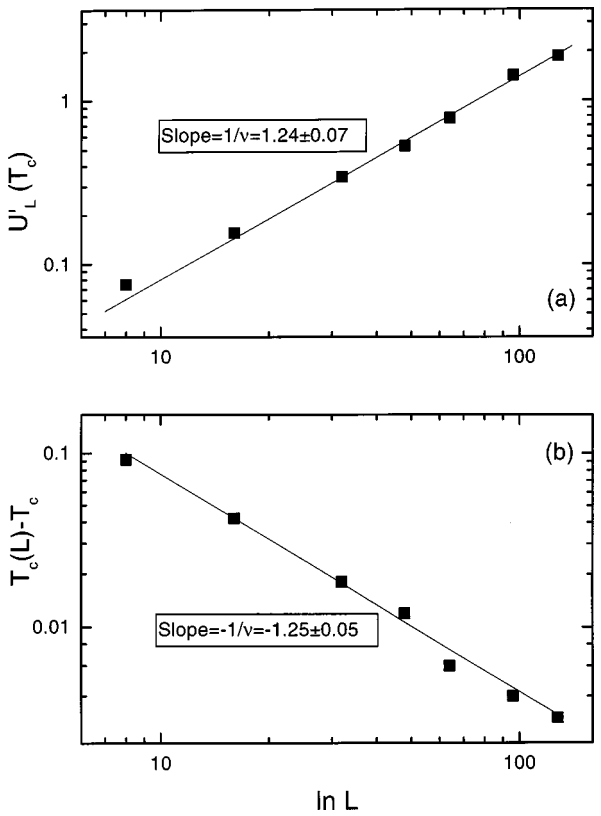

FIG. 5. log-log plots of Monte Carlo data at the disorder to infinite rodlike micelles G_4, for $K_1/K_0=2$ and $J/K_0=0.5$, at $H=-0.4$. The sizes used are $L=8$, 16, 32, 48, 64, 96, and 128. (a) Size dependence of $U_L'(T_c)$ versus L. The straight line is the best fit to the data from linear least-squares method, which gives $\nu=0.806\pm0.07$. (b) Size dependence of $(T_L\text{-}T_c)$ versus L. The straight line is the best fit to the data from linear least-squares method, which gives $\nu=0.80\pm0.05$.

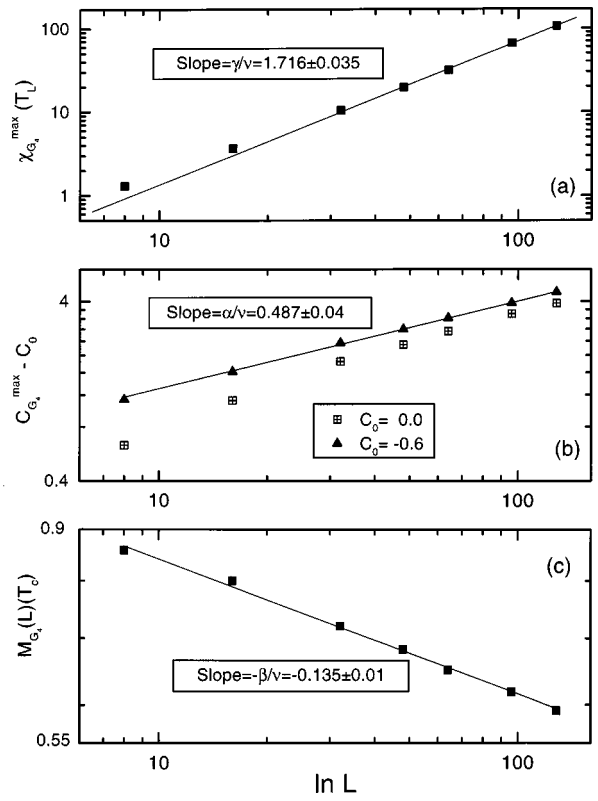

FIG. 6. Finite-size dependence of critical behavior for $K_1/K_0=2$ and $J/K_0=0.5$, at $H=-0.4$ in log-log plots of: (a) The maximum of the order-parameter susceptibility $\chi_{G_4}^{\max}$ versus L. The straight line is the best fit to the data from linear least-squares method which gives $\gamma/\nu=1.716\pm0.035$. (b) The maximum of the divergent part of the specific heat $C_{G_4}^{\max}-C_0$ versus L. The straight line is the best fit to the data from linear least-squares method which gives $\alpha/\nu=0.487\pm0.04$. (c) The infinite rodlike G_4 order parameter at the infinite critical temperature T_c, $MG4_L(T_c)$ versus L. The straight line is the best fit to the data from linear least-squares method, which gives $\beta/\nu=0.135\pm0.01$.

this model. According to the classification of Shick and coworkers based on Landau-Lifshitz theory, the transitions $G_4\leftrightarrow G_1$ and $G_5\leftrightarrow G_6$ belong to the universality class of the *XY* model with cubic anisotropy, whereas the disorder-order $G_{1,6}\leftrightarrow G_2$ and the order-order $G_5\leftrightarrow G_2$ transitions belong to the Ising universality.[43,44] We point out that, in general, when long range interactions are added to the Ising model, a non universal behavior is exhibited by these models.[37,39,41]

(i) For $K_1/K_0=2.0$, $J/K_0=0.5$ to determine the universality of the critical line separating the G_4 structure from the disordered phase, we choose a value of H far from the crossover region, $H=0.0$. We used $H=-0.4$ with long runs and lattices of size up to $L=128$. For $L\leqslant32$ a total of 10^6 MCS were used with the runs decreasing in length with increasing L until for $L=128$ a total of 3×10^5 MCS were kept for the averages. For the precise determination of the infinite critical temperature we used the standard cumulant intersection method.[45] Our estimate of T_c from the crossing of U_L for large L is $T_c=0.958\pm0.001$. With T_c determined, we can now evaluate the critical exponent of the model. From Eq. (18) we see that, at the critical temperature T_c, $U_L'(T_c)$ scales as $L^{1/\nu}$. Then, from a log-log plot of $U_L'(T_c)$ versus L, as can be seen in Fig. 5(a), the best fit to the Monte Carlo data gives us $\nu=0.806\pm0.07$. Another way to find the critical exponent ν is to use the location of the specific-heat peak as the finite lattice critical temperature $T_c(L)$, then $T_c(L)-T_c\approx L^{-1/\nu}$. The result obtained, Fig. 5(b), $\nu=0.8\pm0.05$ is consistent with the previous one.

Also, for sufficiently large values of L, the maximum of the specific heat $C^{\max}-C_0$ with C_0 the nondivergent part of the specific heat and the susceptibility $\chi^{\max}$, should diverge as $L^{\alpha/\nu}$ and $L^{\gamma/\nu}$, respectively. Finally, at T_c the order parameter should go to 0 as $L^{-\beta/\nu}$. Our results are shown in Figs. 6(a)–6(c), the best fits yield $\gamma/\nu=1.716\pm0.035$, $\alpha/\nu=0.486\pm0.04$ with $C_0=-0.6$, the value of C_0 used is the smallest one for which the variation of the entire size range appeared linear, which combined with the hyperscaling relation $d\nu=2-\alpha$ yield $\nu=0.804$, which is in agreement with the previous results of ν, and $\beta/\nu=0.135\pm0.02$, which is in agreement with the universal value of $2\beta/\nu=1/4$. We have also used the same method to find the critical temperature and the exponents (we do not present the plots here) for the $G_5\leftrightarrow G_6$ transition, we have located the critical temperature at $T_c=1.427\pm0.001$, and our best fits give $\nu=0.772\pm0.04$ from Eq. (18) at T_c and $\nu=0.768\pm0.02$ from the analysis of $T_c(L)-T_c$. For the other quantities our best fits are $\gamma/\nu=1.748\pm0.01$, $\alpha/\nu=0.623\pm0.02$ with $C_0=-0.2$ and $\beta/\nu=0.07\pm0.02$. In addition, by assuming the values of the ex-

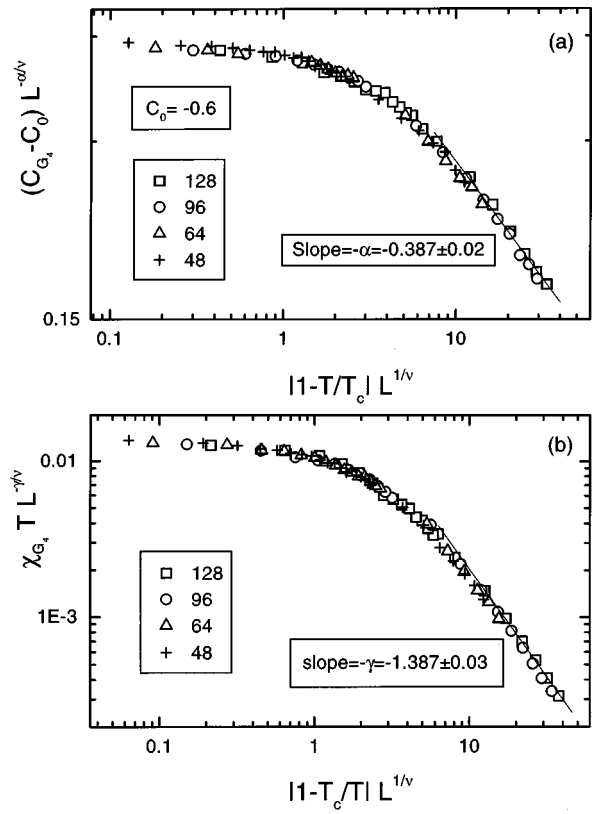

FIG. 7. Finite-size scaling of Monte Carlo data at the disorder to infinite rodlike micelles G_4 for $K_1/K_0=2$ and $J/K_0=0.5$ and at $H/K_0=-0.4$ are shown for (a) the specific heat C_{G_4} and (b) the susceptibility χ_{G_4} in the ordered phase. The critical exponents used are $\nu=0.806$, $\alpha=0.388$, and $\gamma=1.3855$, with $T_c=0.958$.

ponents determined above, we have found good finite-size scaling for large lattices of the specific heat and the susceptibilities in the ordered phase G_4, Figs. 7(a)–7(b) (with $\nu=0.806$, $\alpha=0.388$, $\gamma=1.3855$, $T_c=0.958$, and $C_0=-0.6$), and also in the other ordered phase G_5, figures not shown (with $\nu=0.77$, $\alpha=0.478$, $\gamma=1.3476$, $T_c=1.427$, and $C_0=-0.2$). We note that, we have also performed finite-size scaling for the different quantities C, χ, and M by using the exact values of the exponent $\nu=1.0$, $\beta=0.125$, $\gamma=1.75$, and $\alpha=0$.[37] The plots (not shown) we have obtained are worse than those presented here. All our results, to within the errors in the simulations, are consistent and indicate that these continuous transitions are in the XY model with cubic anisotropy. Since our results of $\gamma/\nu\approx 1.75$, this suggest that Suzuki's weak universality where $\gamma/\nu=7/4$ [Ref. 46], holds for this model.

Transfer-matrix finite-size-scaling results for the thermal exponent ν are obtained with strip widths $N/N'=\frac{4}{8}$ and $\frac{8}{12}$ from Eq. (8) and are presented in Fig. 8. We note that when we approach the crossover region (in the neighborhood of $H=0$) from both the high and the low field the exponent ν is oscillating and decreasing with the strip widths, so we could not conclude about the critical behavior in this region and larger strip widths are needed. Whereas far from this region, ν is varying along these critical lines, even this variation is rather weak. By increasing the magnetic field from both sides, the estimates of ν drop to ones that are close to the Ising tricritical value of 5/9.[47–50] For the points used for MC

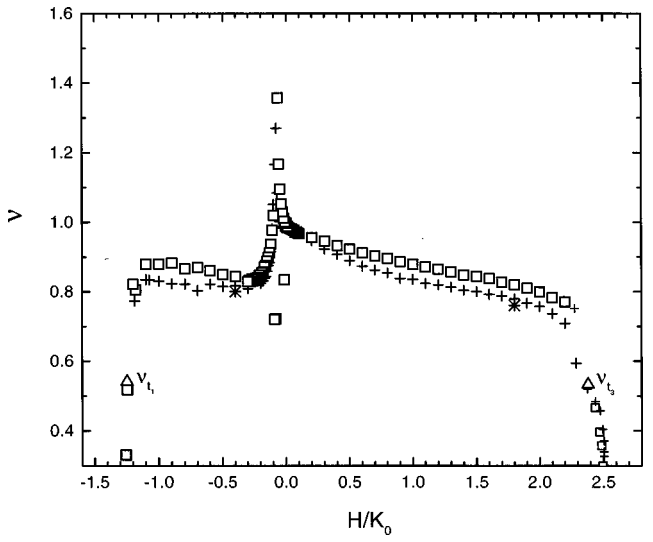

FIG. 8. The critical exponent ν, as obtained from transfer-matrix calculations with $\frac{4}{8}$ and $\frac{8}{12}$ scaling [squares for $N/N'=\frac{4}{8}$ and plus (+) for $\frac{8}{12}$] for $K_1/K_0=2$ and $J/K_0=0.5$ for the critical transitions from the disorder to infinite rodlike micelles and reversed micelles, respectively. Only near the tricritical points C_1 and C_3 the finite-size effects become small, and the $\frac{8}{12}$ estimates for the tricritical values of ν (shown by triangles) are $\nu_{t_1}=0.5412$ and $\nu_{t_3}=0.5325$, also Monte Carlo results are shown by stars (*).

simulations, transfer matrix results yield, $\nu=0.818\pm0.001$ at $H/K_0=-0.4$ and $\nu=0.78\pm0.001$ at $H/K_0=1.8$. Apart from the finite-size effects due to the small sizes used here, the TMFSS and MC results are consistent with each other and confirm that the transitions $G_4\leftrightarrow G_1$ and $G_5\leftrightarrow G_6$ belong to the universality class of the XY model with cubic anisotropy which has nonuniversal variable exponents.

(ii) For $K_1/K_0=0.25$, $J/K_0=1.0$ [Fig. 9] the transfer-matrix estimate of ν for strip widths $N/N'=8/12$ at $H/K_0=0.0$ is $\nu=1.0004\pm0.001$, which is close to the Ising critical value of $\nu=1$ (Refs. 47–50) and by increasing the mag-

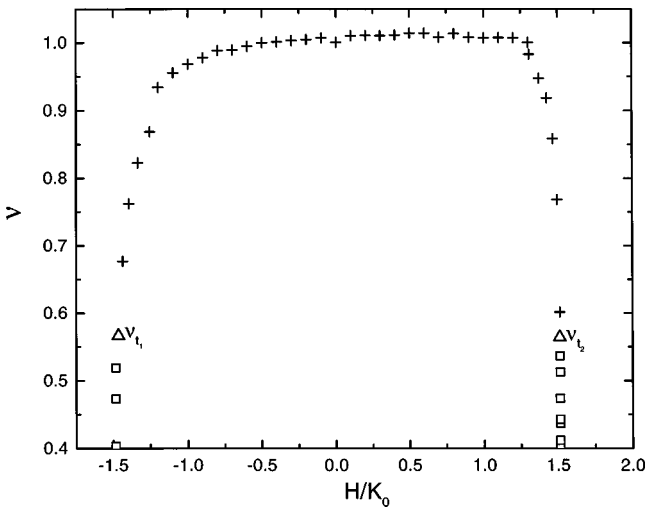

FIG. 9. The critical exponent ν, as obtained from transfer-matrix calculations with $\frac{8}{12}$ scaling (squares) for $K_1/K_0=0.25$ and $J/K_0=1.0$ for the critical transitions from the disorder to spherical micelles G_2. Our $\frac{8}{12}$ estimates for the tricritical values of ν (shown by triangles) are $\nu_{t_1}=0.574$ and $\nu_{t_2}=0.566$.

netic field (in absolute value) in both directions, this value of ν persists until the tricritical points are reached where the estimates of ν drop to ones that are close to the Ising tricritical value of $\frac{5}{9}$. Thus suggesting that the order-disorder transition ($G_1 \leftrightarrow G_2 \leftrightarrow G_6$) belongs to the Ising critical and tricritical universality.

VI. SUMMARY AND CONCLUSION

We have made a thorough study of the multicritical behavior of a lattice-gas model for micellar binary solutions of water and amphiphile that has been proposed by Shnidman and Zia, by using transfer-matrix finite-size scaling and Monte Carlo simulations. Apart from the finite-size effects and the uncertainties in the simulations, the phase diagrams obtained in the magnetic-field-temperature (H,T) plane by these two nonperturbative methods consist of lines of first- and second-order transitions with different multicritical points of higher order and are consistent with each other but are qualitatively better than those obtained by mean-field approximation MFA.[21] The limitation of the MFA is that it ignores fluctuations that are very strong in two dimensions. It predicts the rarefied micelle G_3 at high temperature for $K_1/K_0=2.0$ and $J/K_0=0.5$, thus resulting in a wrong topology of the phase diagram. Also the continuous line separating the disorder from the ordered phase G_2 extends down to $T=0$ for $K_1/K_0=0.25$ and $J/K_0=1.0$ at a high positive magnetic field. Our nonperturbative methods (TMFSS and MC) show the absence of the rarefied micelle G_3 for the former case and the presence of a first-order transition with a tricritical point for the latter case. We have also determined the phase diagrams by TMFSS calculations in the amphiphile concentration-temperature (ρ_s,T) plane. These phase diagrams would provide a rich laboratory for experimental studies, such as the one of Fig. 3(b) that qualitatively resemble, the phase diagram of $C_{12}Na/H_2O$ system. On the other hand, these two nonperturbative methods allow us to understand much more this complicated model by computing the exponents of this model and so to define well its universality class. From TMFSS calculations and large-scale MC simulations, we show that the continuous order-disorder infinite rodlike micelles and reversed micelles to isotropic micellar solutions transitions both belong to the universality class of the *XY*-model cubic anisotropy, which has nonuniversal variable exponents. Thus confirming the nonuniversality scenario of Shnidman for rodlike micelles.[51] Also from TMFSS calculations only, we have shown that the transitions for the disorder-order isotropic micellar solutions to the spherical micellar solid phase and the order-order spherical micellar solid phase to reversed micellar phase both belong to the $d=2$ Ising universality class. All our results are in good agreement with Schick and co-workers classification based on Landau-Lifshitz theory.

Finally, we hope that we have completed the comprehension about this rich model and we believe that this Ising model with multiparticle interactions would be a good candidate for describing the experimental micellar phase diagrams and for the determination of the critical exponents.

ACKNOWLEDGMENTS

One of the authors (S.B.) would like to thank the Abdus-Salam International Center For Theoretical Physics for financial support. He also thanks the hospitality and the computational resources of the center where this work has been completed.

[1] K. A. Dawson and Z. Kurtovic, J. Chem. Phys. **92**, 5473 (1990).
[2] J. W. Halley and A. J. Kolan, J. Chem. Phys. **88**, 3313 (1988).
[3] M. W. Matsen and D. E. Sullivan, Phys. Rev. A **41**, 2021 (1990).
[4] G. Gompper and M. Schick, Chem. Phys. Lett. **163**, 475 (1989).
[5] G. Gompper and M. Schick, *Self-Assembling Amphiphilic Systems in Phase Transitions and Critical Phenomena*, edited by C. Domb and J. L. Lebowitz (Academic, London, 1994), Vol. 16.
[6] *Micelles, Membranes, Microemulsions and Monolayers*, edited by W. M. Gelbart, D. Roux, and A. Ben-Shaul (Springer-Verlag, New York, 1994).
[7] N. Jan and D. Stauffer, J. Phys. (France) **49**, 623 (1988).
[8] *Physics of Amphiphiles: Micelles, Vesicles and Microemulsions*, edited by V. Degiorgio and M. Corti (North-Holland, Amsterdam, 1985).
[9] G. J. T. Tiddy, Phys. Rep. **57**, 1 (1980).
[10] G. Gompper and S. Zschocke, Europhys. Lett. **16**, 731 (1991).
[11] J. M. Seddon, Biochim. Biophys. Acta **1031**, 1 (1990).
[12] H. Hoffmann, Adv. Colloid Interface Sci. **32**, 123 (1990).
[13] R. Strey, R. Schmäcker, D. Roux, F. Nallet, and U. Olsson, J. Chem. Soc., Faraday Trans. **86**, 2253 (1990).
[14] V. Degiorgio, M. Corti, and L. Cantu, Chem. Phys. Lett. **151**, 349 (1988).
[15] J. N. Israelachvili, D. J. Mitchell, and B. W. Ninham, J. Chem. Soc., Faraday Trans. 1 **72**, 1525 (1976).
[16] D. J. Mitchell, G. J. T. Tiddy, L. Warring, Th. Bostock and M. P. Mc Donald, J. Chem. Soc., Faraday Trans. 1 **79**, 975 (1983).
[17] P. Debye and E. W. Anacker, J. Phys. Colloid Chem. **55**, 644 (1951).
[18] G. Gompper and S. Klein, J. Phys. II **2**, 1725 (1992).
[19] Y. Shnidman and R. K. P. Zia, J. Stat. Phys. **50**, 839 (1988).
[20] A. Benyoussef, L. Laanait, and N. Moussa, Phys. Rev. B **48**, 16 310 (1993).
[21] A. Benyoussef, L. Laanait, N. Masaif, and N. Moussa, J. Phys.: Condens. Matter **8**, 3347 (1996).
[22] A. Benyoussef, L. Laanait, N. Masaif, and N. Moussa, J. Phys. I **6**, 1043 (1996).
[23] N. Moussa, Y. El Amraoui, S. Bekhechi, A. Benyoussef, and L. Laanait, following paper, Phys. Rev. B **61**, 3372 (2000).
[24] P. A. Rikvold, K. Kaski, J. D. Gunton, and M. C. Yalabik, Phys. Rev. B **29**, 6285 (1984).
[25] W. Kinzel and M. Shick, Phys. Rev. B **23**, 3435 (1981).
[26] N. C. Bartelt, T. L. Einstein, and L. D. Roelofs, Phys. Rev. B **34**, 1616 (1986).
[27] L. D. Roelofs, T. L. Einstein N. C. Bartelt, and J. D. Shore, Surf. Sci. **176**, 295 (1986).
[28] J. D. Kimel, S. Black, P. Carter, and Y. L. Wang, Phys. Rev. B **35**, 3347 (1987).
[29] J. D. Kimel, P. A. Rikvold, and Y. L. Wang, Phys. Rev. B **45**, 7237 (1992).

[30] S. Bekhechi and A. Benyoussef, Phys. Rev. B **56**, 13 954 (1997), and references therein.
[31] M. P. Nightingale, Physica A **83**, 561 (1976); Phys. Lett. **59A**, 486 (1977); M. P. Nightingale, J. Appl. Phys. **53**, 7927 (1982).
[32] C. Domb, Adv. Phys. **9**, 149 (1960).
[33] P. D. Beale, Phys. Rev. B **33**, 1717 (1986).
[34] P. A. Rikvold, W. Kinzel, J. D. Gunton, and K. Kaski, Phys. Rev. B **28**, 2686 (1983).
[35] P. A. Rikvold, Phys. Rev. B **32**, 4756 (1985).
[36] P. A. Rikvold, Phys. Rev. B **33**, 6523 (1986).
[37] T. Aukrust, M. A. Novotny, P. A. Rikvold, D. P. Landau, Phys. Rev. B **41**, 8772 (1990), and references therein.
[38] *Applications of the Monte Carlo Method in Statistical Physics*, edited by K. Binder (Springer Verlag, Berlin, 1988).
[39] K. Binder and D. P. Landau, Phys. Rev. B **21**, 1941 (1080).
[40] M. E. Fisher, in Proceedings of the International School of Physics ''Enrico Fermi,'' Course LI, Varenna, 1970, edited by M. S. Green (Academic, New York, 1971), p. 1.
[41] M. Badehdah, S. Bekhechi, A. Benyoussef, and M. Touzani, Eur. Phys. J. B **4**, 431 (1998).
[42] C. Madelmont and R. Perron, Colloid Sci. **254**, 581 (1976).
[43] E. Domany, M. Schick, J. S. Walker, and R. B. Griffiths, Phys. Rev. B **18**, 2209 (1978).
[44] M. Schick, Prog. Surf. Sci. **11**, 245 (1981).
[45] K. Binder, Z. Phys. B **43**, 1197 (1981).
[46] M. Suzuki, Prog. Theor. Phys. **51**, 1992 (1974).
[47] H. E. Stanley, *Introduction to Phase Transitions and Critical Phenomena* (Oxford University Press, Oxford, 1971).
[48] B. M. McCoy and T. T. Wu, *The Two-Dimensional Ising Model* (Harvard University Press, Cambridge, MA, 1973).
[49] M. P. M. den Nijs, J. Phys. A **12**, 1857 (1979).
[50] B. Nienhuis, E. K. Riedel, and M. Schick, J. Phys. A **13**, L189 (1980).
[51] Y. Shnidman, Phys. Rev. Lett. **56**, 201 (1986); **56**, 2546 (1986); **58**, 621 (1987).